Journal of Alloys and Compounds 509 (2011) 7798–7802

Contents lists available at ScienceDirect

Journal of Alloys and Compounds

journal homepage: www.elsevier.com/locate/jallcom

Application of $^{n}Bu_2Sn(acac)_2$ for the deposition of nanocrystallite SnO_2 films: Nucleation, growth and physical properties

Yinzhu Jiang[a], Wenping Sun[c], Mi Yan[a,*], Naoufal Bahlawane[b]

[a] State Key Laboratory of Silicon Materials, Department of Materials Science and Engineering, Zhejiang University, Hangzhou 310027, China
[b] Department of Chemistry, Bielefeld University, Universitaetsstr. 25, 33615 Bielefeld, Germany
[c] CAS Key Laboratory of Materials for Energy Conversion, Department of Materials Science and Engineering, University of Science and Technology of China (USTC), Hefei, 230026, China

ARTICLE INFO

Article history:
Received 4 March 2011
Received in revised form 2 May 2011
Accepted 3 May 2011
Available online 12 May 2011

Keywords:
Tin oxide
Films
Nucleation and growth
Precursor
CVD

ABSTRACT

High-quality uniform SnO_2 thin films were successfully prepared by pulsed-spray evaporation chemical vapor deposition (PSE-CVD) method, using a cost-efficient precursor of $^{n}Bu_2Sn(acac)_2$. The volatility and stability of $^{n}Bu_2Sn(acac)_2$ were studied through thermogravimetric-differential thermal (TG-DTA) analysis and mass spectrometry, indicating the good adaptability for the CVD process. Deposition of SnO_2 films was made in the range of 250–450 °C to investigate the effect of substrate temperature on their structural and physical properties. The film growth activation energy changes from 66.5 kJ/mol in the range of 250–330 °C to 0 kJ/mol at 330–450 °C, suggesting the change of the rate-limiting step from surface kinetics to diffusion control. All films possess the rutile-type tetragonal structure, while a change of preferred orientation from (1 1 0) to (1 0 1) plane is observed upon the increase of the deposition temperature. The different variation of the nucleation and growth rates with the deposition temperature is proposed to explain the observed unusual change of crystallite size. A significant deterioration of the electrical conductivity was observed upon the increase of the deposition temperature, which was tentatively attributed to the non-specific decomposition of the precursor at high temperature leading to carbon contamination. Optical measurements show transparencies above 80% in the visible spectral range for all films, while band gap energy increases from 4.02 eV to 4.08 eV when the deposition temperature was raised from 250 °C to 450 °C.

1. Introduction

As one of the most widely exploited metal oxides, tin oxide (SnO_2) has attracted a considerable attention due to its unique physical and chemical properties, such as wide band gap, good chemical stability, high electrical conductivity and excellent functionality [1–6]. Uniform SnO_2 films are particularly useful for gas sensing, solar cells and nanoelectronic devices, since the uniformity of films is crucial for minimizing current leakage in device applications.

It is well accepted that the physicochemical properties of functional films strongly depend on the selected preparation method [7]. Up to date, various physical and chemical techniques have been utilized to prepare SnO_2-based films, including chemical vapor deposition (CVD), sputtering, thermal evaporation, pulsed laser deposition (PLD), ion-beam deposition, spin-coating and sol–gel [8–18]. Some of these techniques are usually associated with the necessity of high temperatures either during deposition or during a post-deposition annealing, which damages the surface of the films and negatively effects on the optical properties [19]. CVD is a universal technique that was widely used in the deposition of SnO_2 either in experimental research or industrial processes [20].

In a conventional CVD process, gaseous precursors are transported to a heated substrate on which they react yielding a solid film on the substrate. Naturally, the volatility and decomposition mechanism of a precursor largely determine the final quality and physical properties of the films [21]. Various types of precursors have been applied in the deposition of SnO_2 films, including $SnCl_4$, $Sn(NO_3)_4$, dimethyltindichloride ($((CH_3)_2SnCl_2$, DMTC), monobutyltintrichloride (n–$C_4H_9SnCl_3$, MBTC), Me_4Sn, Et_4Sn, $Me_2Sn(NMe)_2$, $Bu_2Sn(O_2CMe)_2$, $Sn(O_2CMe)_2$, and $Sn(NMe)_2$ [22]. Inorganic precursors generally need high deposition temperature and tend to result in halide contaminations, while organometallic precursors are air/moisture-sensitive, toxic and/or quite expensive [21,22]. Therefore, exploring the suitability of volatile and liquid metal-organic potential precursors is very important for the development of SnO_2-based films.

In the present study, we provide for the first time an evaluation of the suitability of $^{n}Bu_2Sn(acac)_2$

* Corresponding author. Tel.: +86 57187952730; fax: +86 57187952366.
E-mail address: mse_yanmi@zju.edu.cn (M. Yan).

0925-8388/$ – see front matter © 2011 Elsevier B.V. All rights reserved.
doi:10.1016/j.jallcom.2011.05.014

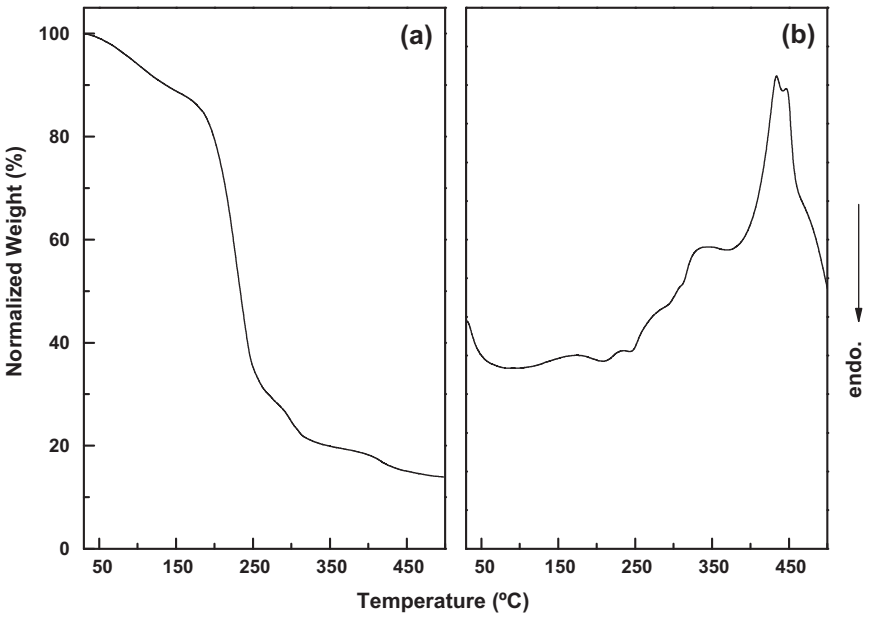

Fig. 1. Thermal analysis curves for $^{n}Bu_2Sn(acac)_2$ in air, 10 °C/min: (a) TG curve; and (b) DTA curve.

$((n\text{–}C_4H_9)_2Sn(CH_3COCHCOCH_3)_2)$ as a precursor for the chemical vapor deposition of SnO_2 films. This potential precursor is a cost-effective liquid source with sufficient volatility and is conveniently air/moisture stable and non-toxic. The thermal behavior of the precursor was examined by thermogravimetric-differential thermal analysis (TG-DTA) and mass spectrometry (MS). The structural, electrical and optical properties of SnO_2 films were investigated as a function of deposition temperature, with the consideration of the nucleation and growth processes.

2. Experimental

The schematic set-up of the pulsed-spray evaporation chemical vapor deposition (PSE-CVD) apparatus for the growth of SnO_2 thin films was described elsewhere [7]. This process runs in a pulsed way by injecting a liquid feedstock in the form of a spray, which is an innovative technique for the fabrication of metal and metal oxide films [2,7,23–25]. The deposition was performed in the range of 250–450 °C on glass substrates. In this set-up, the evaporation and transport zones were set above the cold-wall CVD chamber, the temperatures of which were kept at 180 °C for the evaporation and 210 °C for the transport of the precursor. The $^{n}Bu_2Sn(acac)_2$ (Strem chemical) compound was dissolved in ethanol at a concentration of 2.5 mmol/L and used as a liquid feedstock, which was introduced into the evaporation section as a spray in a pulsed mode (pulse width: 25 ms, pulsing frequency: 1 Hz) with an average delivery rate of 1.50 mL/min. N_2 (225 sccm) and O_2 (750 sccm) flows were used as carrier and reaction gases, respectively. The working pressure in the reactor during deposition was stabilized at 50 mbar.

The precursor was characterized by TG-DTA, which was conducted in air flow of 80 mL/min at ambient pressure, with a heating rate of 10 °C/min from 40 °C to 500 °C using TG/Shimadzu TGA-50H and DTA/Shimadzu DTA-50. A mass spectrometer (Agilent 6890/Micromass GCT-MS) was used to analyze the gas-phase species released from $^{n}Bu_2Sn(acac)_2$ when heated in vacuum at the rate of 10 °C/min from 150 °C to 400 °C. The sampled gas was ionized by electron impact (EI) and the mass was scanned up to 800 *m/z*. X-ray diffraction (XRD) patterns of the grown films were recorded with a Philips X'Pert Pro MDR X-ray diffractometer, using Cu Kα radiation. The thickness of the grown films was estimated gravimetrically with a precision microbalance and assuming the full density of SnO_2. The so-determined nominal thickness was kept around 190 nm for all films deposited at different temperatures. The electrical conductivity measurements were performed in air atmosphere at room temperature using a four-probe d.c. equipment. The optical transmittance and absorption were measured with a Shimadzu UV-5001PC UV–visible spectrophotometer in the wavelength range of 300–900 nm.

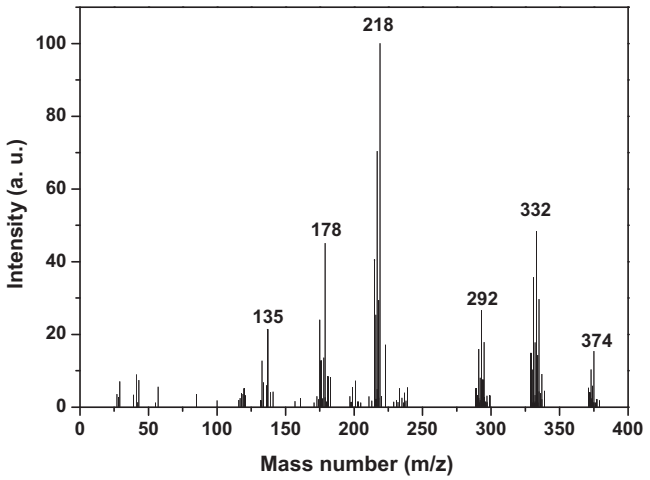

Fig. 2. Typical mass spectrum of $^{n}Bu_2Sn(acac)_2$ taken at 200 °C.

3. Results and discussion

3.1. Volatility and stability of $^{n}Bu_2Sn(acac)_2$

In order to obtain the optimal deposition conditions and provide useful information regarding the thermal behavior, the $^{n}Bu_2Sn(acac)_2$ precursor was analyzed by TG-DTA in air, as shown in Fig. 1. Since $^{n}Bu_2Sn(acac)_2$ is liquid at room temperature, it evaporates steadily with the temperature increase. Nevertheless, increasing the temperature above 200 °C induces a steep weight loss, Fig. 1a, that corresponds to a series of exothermal processes as shown in Fig. 1b. These results show that the precursor evaporates much more quickly since the temperature of 200 °C is above the boiling point. Worthy of noting is that there is a high residual amount as 15% of the initial weight and meanwhile a sharp exothermic peak around 450 °C in the DTA curve, which represents decomposition and oxidation of the sample [26] and might cause the organic residues in the films. Therefore, film deposition at high temperatures might induce carbon/organic contamination. In our case, the temperature of the evaporation zone was set around 200 °C, which favors the evaporation without decomposition in the gas-phase. The acquired mass spectrum at 200 °C, Fig. 2, shows that the precursor is still dominantly intact, with the presence of six major peaks at $m/z = 375$, 332, 292, 218, 178 and 135, corresponding to $^{+}C_4H_9Sn(acac)_2$, $^{+}CH_3Sn(acac)_2$,

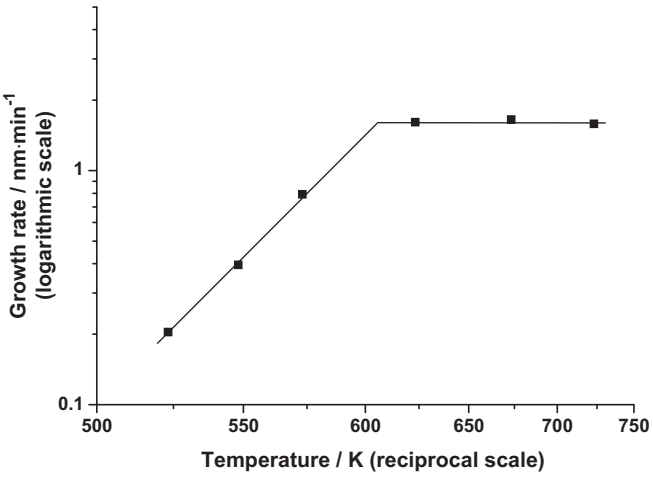

Fig. 3. The Arrhenius plot of the deposition rate.

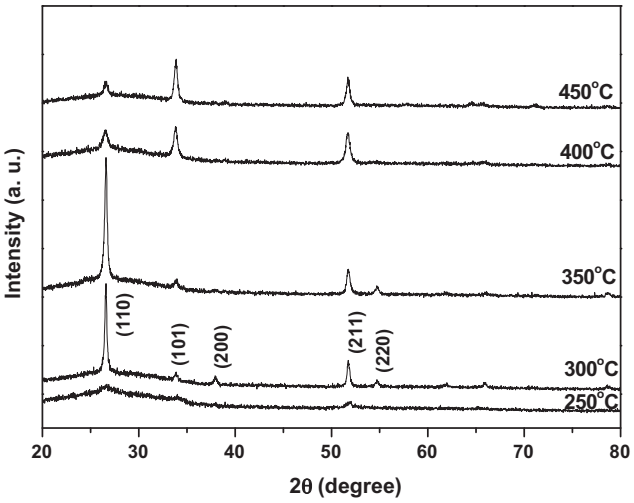

Fig. 4. XRD patterns of as-deposited SnO_2 films obtained at different substrate temperatures.

$^{+}CH_3Sn(acac)_2COC_3H_7$, $^{+}Sn(acac)_2$, $^{+}SnCOC_3H_7$, and ^{+}SnO respectively.

3.2. Growth kinetics of SnO_2 films

The effect of the substrate temperature on the growth rate was investigated using glass substrates in the range of 250–450 °C. The deposition rate (r) was dramatically enhanced from 0.2 to 1.6 nm/min when the substrate temperature was increased from 250 to 350 °C. Deposition rate complies well with the Arrhenius law, $r = A\exp(-E_a/RT)$, where A, E_a, R and T are a constant, the apparent activation energy, the gas constant and the substrate absolute temperature, respectively. The Arrhenius plot of the deposition rate, Fig. 3, indicates two different deposition regimes. In the low-temperature regime (<330 °C), the deposition takes place with an apparent activation energy of 66.5 kJ/mol, which is likely to correspond to the kinetically controlled growth mode. The growth rate is almost temperature-independent above 330 °C indicating transport limitations. The surface kinetic processes become so rapid that the deposition process became limited by the diffusion of the active gaseous species through the boundary layer.

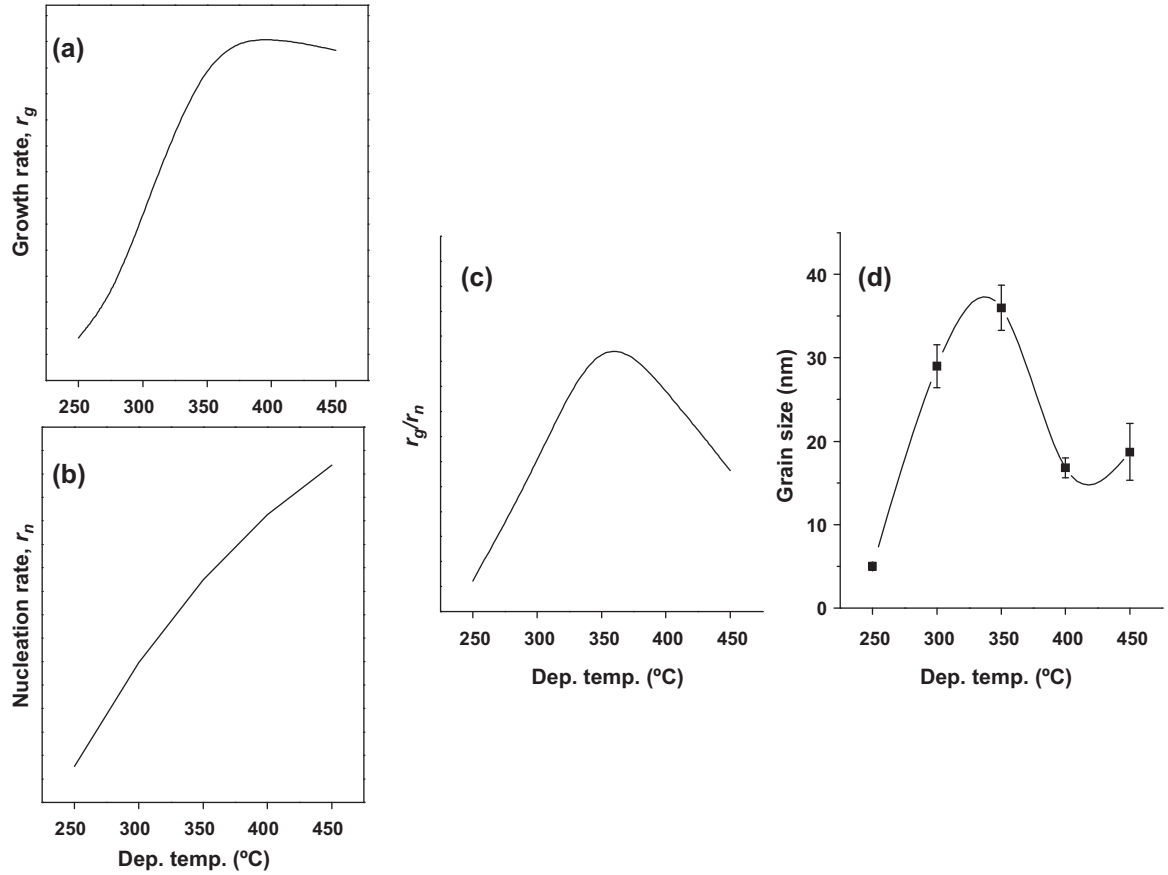

Fig. 5. Effect of deposition temperature on the growth rate (a), nucleation rate (b), r_g/r_n (c) and crystallite size (d).

3.3. Effect of nucleation and growth processes on the characteristics of the grown films

The nucleation and growth process also play a key role on the corresponding structural and morphological properties of SnO_2 films. Fig. 4 shows the XRD patterns of the obtained 190 nm-thick SnO_2 films at substrate temperatures in the range of 250–450 °C. All films were identified as rutile-type SnO_2 (JCPDS #88-0287). The limited surface diffusion of the precursors at 250 °C prevents the further growth of the formed growth nuclei, which justifies the poor crystallinity of films obtained at this temperature. The XRD pattern of the grown film at 300 °C exhibits intense diffraction peaks suggesting the enhanced crystallinity. Generally, the acquired XRD patterns show a preferred (1 1 0) orientation of films grown below 400 °C, which leads to the exposure of the face with low surface energy. Nevertheless, an excessive thermal activation enables the formation of surfaces with higher energies (1.29 J/m^2 for (1 1 0) and 1.6 J/m^2 for (1 0 1)) [1].

Using the Scherrer equation, $d = 0.89\lambda/(B\cos\theta)$, where d, λ, B, and θ are respectively the crystallite size, X-ray wavelength, the full-width-at-half-maximum height and Bragg angle, the variation of the crystallite size was determined, giving more information about the nucleation and growth process, as shown in Fig. 5d. The crystallite size undergoes an abnormal change with the increase of deposition temperature. From 250 to 350 °C, the crystallite size increases from 5 nm to 38 nm. However when the deposition temperature increases further, the crystallite size decreases dramatically to around 18 nm, which contrasts with the usually observed continuous increase of crystallite size with the temperature [7]. The temperature dependency of the nucleation (r_n) and growth (r_g) rates might be the primary reason for this behavior. Whereas the nucleation step is necessary for the growth of crystallite films, an excessively high nucleation rate relative to the growth rate disturbs the growth process and leads to the formation of films with poor crystallinity and small crystallite size. In the present case, the growth rate increases continuously from 250 to 350 °C and then reaches a constant value at higher temperatures (Fig. 5a), while the nucleation rate is expected to increase steadily in the entire range of deposition temperature (Fig. 5b). With this assumption, the further growth of individual nuclei, expressed as r_g/r_n, is then expected to follow the trend sketched in Fig. 5c, which is similar with that of crystallite size. That is to say, in the low-temperature range the further growth of nuclei increases faster with the temperature then the rate of nucleation, which results in the increase of crystallite size. Above 350 °C, however, the nucleation rate predominates, leading to the decrease of crystallite size.

3.4. Electrical and optical properties of SnO_2 films

Fig. 6 shows the variation of electrical resistivity of the as-grown SnO_2 films on glass substrates at different deposition temperatures. Films deposited at 250 °C show the lowest electrical resistivity that lies at 0.21 Ω cm. With the increase of deposition temperature, the electrical resistivity gradually increased to reach a value that is 35 fold higher at 450 °C. It is worth noting that the evolution of the crystallite size with the temperature shows a maximum at 350 °C, and the SEM surface inspection did not show any significant morphological impact of the growth temperature. Therefore, the trend of the electrical resistivity is unlikely to be related to the structure/texture variations. The most likely cause of the degraded electrical conductivity of films obtained at higher temperature is the presence of carbon impurities, which is indicated in the discussion of TG-DTA part.

The transmission spectra of SnO_2 films deposited at 300–450 °C are shown in Fig. 7a. The measurements were conducted in the wavelength range of 300–900 nm at room temperature using glass substrate as background. In general the average transmittance in the visible spectral range is above 80%. There are no evident differences observed for films deposited at different temperatures, except for the shift of the absorption edge. The detailed optical band gap of E_g for the direct transition was determined from the following equation, $(\alpha h\upsilon)^2 = B(h\nu - E_g)$ where α is the absorption

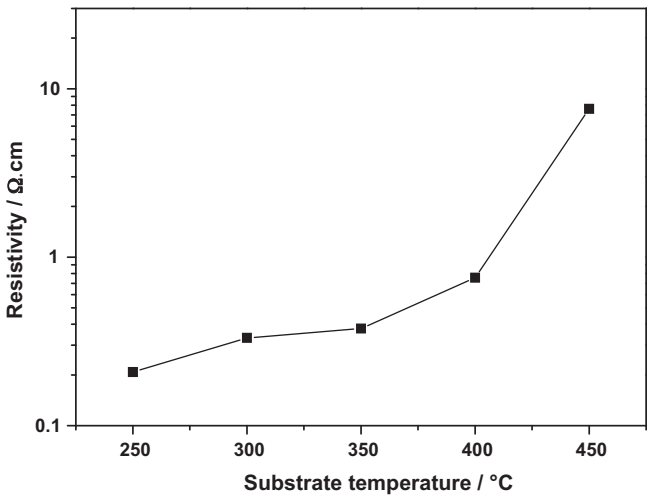

Fig. 6. Resistivity SnO_2 films as a function of deposition temperature.

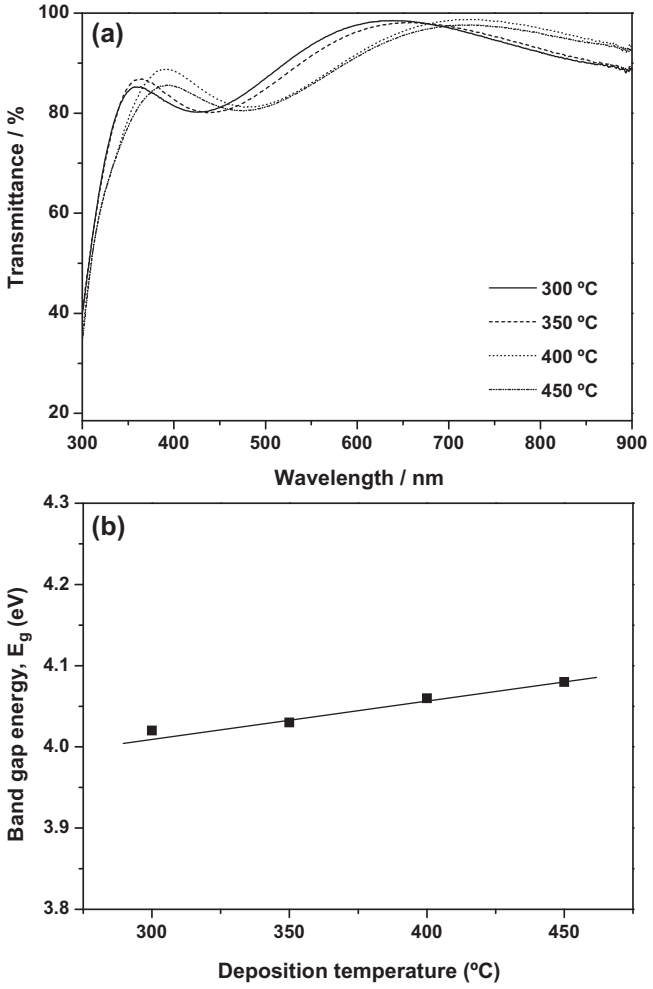

Fig. 7. (a) The transmission spectra of SnO_2 films deposited on glass substrate at different substrate temperatures; (b) Band gap energy E_g vs deposition temperature.

coefficient, B is a material-specific constant, and $h\nu$ is the incident photon energy. Fig. 7b shows the extracted band gap energies using Tauc plots. It is noted that E_g increases from 4.02 eV to 4.08 eV with the increase of deposition temperature. These values exhibit an almost 0.5 eV blue shift from that of bulk SnO_2 (3.6 eV), which might be associated with the incorporation of contaminants in the films as a results of high temperature decomposition of the precursor. Relative to the electrical resistivity, the optical properties of the SnO_2 films are less sensitive to the growth temperature; nevertheless a steady trend is observed in both cases which rules out their correlation with the crystallite size. The obtained result corroborates with the incorporation of carbon contamination into the film upon the less selective decomposition at high temperature. Therefore, the suitability of $^nBu_2Sn(acac)_2$ for the application as precursor for the thermal CVD is restricted to low growth temperatures.

4. Conclusions

Uniform nanocrystallite SnO_2 thin films were successfully prepared at 250–450 °C by PSE-CVD technique, using $^nBu_2Sn(acac)_2$ as precursor. The TG-DTA analysis and mass spectrometry suggest the good volatility and stability of $^nBu_2Sn(acac)_2$, properties that are advantageous for potential CVD precursors. The film growth activation energy changes from 0 kJ/mol to 66.5 kJ/mol at 330 °C with decreasing deposition temperature, indicating the rate-limiting step changing from diffusion control mode to surface kinetics control one. Films deposited at different temperatures show a rutile-type tetragonal structure based on XRD patterns, while the increase of deposition temperature could activate the growth of crystallite planes with different surface energies, leading to the change of preferred orientation. The difference of nucleation rate and growth rate is thought to be the main reason for the change of crystallite size. The electrical resistivity was found to increase from 0.21 Ω cm to 7.58 Ω cm when the deposition temperature was increased from 250 to 450 °C, which might be associated with the increased carbon impurities for films deposited at high temperature. Optical measurements show that all films are largely transparent in the visible spectral region, with an average transparency of 90%. The band gap energy increases from 4.02 eV to 4.08 eV when the deposition temperature increases from 300 to 450 °C.

Acknowledgments

Yinzhu Jiang thanks to the support of Zijin Program of Zhejiang University. The authors express their gratitudes to Prof. Katharina Kohse-Höinghaus for her helpful suggestion and discussions.

References

[1] M. Batzill, U. Diebold, Prog. Surf. Sci. 79 (2–4) (2005) 47.
[2] Y.Z. Jiang, N. Bahlawane, Phys. Chem. Chem. Phys. 13 (2011) 5760.
[3] M. Fang, L.D. Zhang, X.L. Tan, X.Y. Hu, W.W. Yan, P.S. Liu, J. Phys. Chem. C 113 (22) (2009) 9676.
[4] J. He, Q.Z. Cai, F. Xiao, X.W. Lie, W. Sun, X. Zhao, J. Alloys Compd. 509 (2011) L11.
[5] Y.H. Lin, M.W. Huang, C.K. Liu, J.R. Chen, J.M. Wu, H.C. Shih, J. Electrochem. Soc. 156 (11) (2009) K196.
[6] A.R. Babar, S.S. Shinde, A.V. Moholkar, K.Y. Rajpure, J. Alloys. Compd. 505 (2011) 743.
[7] Y.Z. Jiang, N. Bahlawane, J. Phys. Chem. C 114 (11) (2010) 5121.
[8] M. Kwoka, L. Ottaviano, J. Szuber, Thin Solid Films 515 (23) (2007) 8328.
[9] Z. Remes, M. Vanecek, H. Yates, P. Evans, D. Sheel, Thin Solid Films 517 (23) (2009) 6287.
[10] J. Sundqvist, J. Lu, M. Ottosson, A. Harsta, Thin Solid Films 514 (1–2) (2006) 63.
[11] N.F.H. Samad Bazargan, D. Pradhan, K.T. Leung, Cryst. Growth Des. 11 (2011) 247.
[12] E. Manea, E. Budianu, M. Purica, C. Podaru, A. Popescu, I. Cernica, F. Babarada, C. Parvulescu, Romanian J. Inf. Sci. Technol. 10 (1) (2007) 25.
[13] R. Choudhary, S. Ogale, S. Shinde, V. Kulkarni, T. Venkatesan, K. Harshavardhan, M. Strikovski, B. Hannoyer, Appl. Phys. Lett. 84 (9) (2004) 1483.
[14] S.H. Kim, N.M. Park, T.Y. Kim, G.Y. Sung, Thin Solid Films 475 (1–2) (2005) 262.
[15] T. Ohgaki, R. Matsuoka, K. Watanabe, K. Matsumoto, Y. Adachi, I. Sakaguchi, S. Hishita, N. Ohashi, H. Haneda, Sens. Actuators B 150 (1) (2010) 99.
[16] S.Y. Ho, A.S.W. Wong, G.W. Ho, Cryst. Growth Des. 9 (2) (2009) 732.
[17] L.Y. Liang, Z.M. Liu, H.T. Cao, Z. Yu, Y.Y. Shi, A.H. Chen, H.Z. Zhang, Y.Q. Fang, X.L. Sun, J. Electrochem. Soc. 157 (6) (2010) H598.
[18] W.C. Chang, S.C. Lee, X.D. Qi, J. Electrochem. Soc. 157 (7) (2010) J245.
[19] R. Khandelwal, A. Singh, A. Kapoor, S. Grigorescu, P. Miglietta, N. Stankova, A. Perrone, Opt. Laser Technol. 41 (1) (2009) 89.
[20] A.C. Jones, M.L. Hitchman, Chemical Vapour Deposition: Precursors Processes and Applications, RSC Publishing, 2009.
[21] Y. Jiang, M. Liu, Y. Wang, H. Song, J. Gao, G. Meng, J. Phys. Chem. A 110 (50) (2006) 13479.
[22] K. Molloy, J. Chem. Res. 10 (2008) 549.
[23] P.H.T. Ngamou, N. Bahlawane, Chem. Mater. 22 (2010) 4158.
[24] N. Bahlawane, P.A. Premkumar, Z.Y. Tian, X. Hong, F. Qi, K. Kohse-Hoinghaus, Chem. Mater. 22 (2010) 92.
[25] N. Bahlawane, P.H.T. Ngamou, V. Vannier, T. Kottke, J. Hberle, K. Kohse-Hoinghaus, Phys. Chem. Chem. Phys. 11 (2009) 9224.
[26] Y.Z. Jiang, H.Z. Song, L. Li, W.T. Bao, G.Y. Meng, J. Cryst. Growth 267 (2004) 256.